

Contents lists available at ScienceDirect

#### Petroleum Science

journal homepage: www.keaipublishing.com/en/journals/petroleum-science



#### Original Paper

## Exploring *in-situ* combustion effects on reservoir properties of heavy oil carbonate reservoir



Aliya Mukhametdinova <sup>a, \*</sup>, Tagir Karamov <sup>a</sup>, Strahinja Markovic <sup>a</sup>, Andrey Morkovkin <sup>a</sup>, Aleksander Burukhin <sup>a</sup>, Evgeny Popov <sup>a</sup>, Zi-Qi Sun <sup>b</sup>, Ren-Bao Zhao <sup>b</sup>, Alexey Cheremisin <sup>a</sup>

- <sup>a</sup> Skolkovo Institute of Science and Technology (Skoltech), Sikorskogo 11, Moscow, 121205, Russia
- b State Key Laboratory of Petroleum Resources and Engineering, China University of Petroleum (Beijing), Beijing, 102249, China

#### ARTICLE INFO

# Article history: Received 27 December 2023 Received in revised form 11 March 2024 Accepted 28 April 2024 Available online 7 May 2024

Edited by Meng-Jiao Zhou

Keywords: In-situ combustion Thermal EOR Carbonates Porosity and pore size MicroCT NMR SEM CO<sub>2</sub> storage

#### ABSTRACT

Laboratory modeling of *in-situ* combustion is crucial for understanding the potential success of field trials in thermal enhanced oil recovery (EOR) and is a vital precursor to scaling the technology for field applications. The high combustion temperatures, reaching up to 480 °C, induce significant petrophysical alterations of the rock, an often overlooked aspect in thermal EOR projects. Quantifying these changes is essential for potentially repurposing thermally treated, depleted reservoirs for CO<sub>2</sub> storage.

In this study, we depart from conventional combustion experiments that use crushed core, opting instead to analyze the thermal effects on reservoir properties of carbonate rocks using consolidated samples. This technique maintains the intrinsic porosity and permeability, revealing combustion's impact on porosity and mineralogical alterations, with a comparative analysis of these properties pre- and post-combustion. We characterize porosity and pore geometry evolution using low-field nuclear magnetic resonance, X-ray micro-computed tomography, and low-temperature nitrogen adsorption. Mineral composition of the rock and grain-pore scale alterations are analyzed by scanning electron microscopy and X-ray diffraction.

The analysis shows a significant increase in carbonate rocks' porosity, pore size and mineral alterations, and a transition from mixed-wet to a strongly water-wet state. Total porosity of rock samples increased in average for 15%–20%, and formation of new pores is registered at the scale of 1–30  $\mu$ m size. High-temperature exposure results in the calcite and dolomite decomposition, calcite dissolution and formation of new minerals—anhydrite and fluorite. Increased microporosity and the shift to strongly water-wet rock state improve the prospects for capillary and residual CO<sub>2</sub> trapping with greater capacity. Consequently, these findings highlight the importance of laboratory *in-situ* combustion modeling on consolidated rock over tests that use crushed core, and indicate that depleted combustion stimulated reservoirs may prove to be viable candidates for CO<sub>2</sub> storage.

© 2024 The Authors. Publishing services by Elsevier B.V. on behalf of KeAi Communications Co. Ltd. This is an open access article under the CC BY license (http://creativecommons.org/licenses/by/4.0/).

#### 1. Introduction

The *in-situ* combustion is a thermal method of enhanced oil recovery (EOR) based on the use of energy obtained by partial combustion of heavy fractions of oil (coke) in reservoir conditions when an oxidizer (air) is injected from the surface (Burger, 1972). *In-situ* combustion (ISC) is a thermal recovery method that was first conceptualized in the 1920s. It offers numerous advantages, such as improved mobilization of heavy oil and enhanced sweep efficiency,

other secondary and tertiary recovery methods (Nelson and McNeil, 1961). Despite its merits, the field implementation of this method is rather complex, mainly due to uncertainties in efficiency, elevated operational costs, and limited control over combustion front propagation (Manrique et al., 2007). From the 1950s to the late 1990s, approximately 230 ISC pilot projects were conducted in the United States, of which only 37 were considered successful. However, in the 21st century, the ISC process has been revamped and successfully implemented in China, the US, and Canada (Minakov et al., 2023).

which theoretically can yield higher oil recovery rates compared to

Apart from the Middle East, a considerable fraction of global hydrocarbon reserves resides in carbonate reservoirs. These

E-mail address: a.mukhametdinova@skoltech.ru (A. Mukhametdinova).

<sup>\*</sup> Corresponding author.

geological formations are characterized by pronounced heterogeneity, a feature that frequently constrains the efficacy of various enhanced oil recovery techniques (Mogensen and Masalmeh, 2020). For instance, literature reports show that gas injection methods in carbonate formations is challenging poor sweep efficiency, gravity override, and viscous fingering, and often lead to an unfavorable mobility ratio and premature gas breakthrough (Mogensen and Masalmeh, 2020), On the other end, for low-salinity polymer flooding, reports quote optimizing pH and ion composition  $(SO_4^{2-}$  and  $Ca^{2+})$  to control polymer adsorption and wettability alteration as principal issues that have differing effects on permeability and residual oil saturation depending on the ionic environment. In ISC, however, combustion front propagates through the reservoir, reducing the oil viscosity and improving both vertical and horizontal sweep efficiency. Also, as the heavier oil fractions are consumed in this process as a fuel for oxidation, the oil is being upgraded where low-carbon fractions and hydrogen are emitted (Rodriguez et al., 2023). Another aspect is the release of CO<sub>2</sub> resulting from the decomposition of the rock increasing the void space, which may improve reservoir permeability (Bogdanov et al., 1990). In addition, when CO<sub>2</sub> dissolves into oil, it significantly reduces the viscosity, improving oils' overall mobility. But at the same time, excessive gas release in reservoir conditions may suppress the combustion front.

The downsides of ISC application to carbonate fields include the thermal decomposition of carbonate minerals, the formation of chemical deposits which can cause pore blocking and reduction of permeability, and increased risk of excess fracturing (Sarathi, 1999). To study the response of reservoir to ISC process, laboratory screening is required in reservoir conditions. This involves conducting experiments in the high pressure and temperature (HPHT) reactors. These types of experiments provide insight into the key factors controlling the success of the ISC project, such as reaction kinetics, stoichiometry, ignition temperatures, oxidation pathways and optimal injection rates (Khakimova et al., 2020; Mamora et al., 1993; Hascakir and Kovscek, 2014).

For the most rigorous emulation of *in-situ* combustion dynamics under reservoir conditions, pysical models are employed, integrating authentic samples of both reservoir rock and fluids (Burger, 1972). The experiments are typically structured into three phases: the study commences with an exhaustive initial analysis of core, fluid, and gas samples. The second phase involves the in-situ combustion experiment itself, during which the temperature profiles and output curves of gas and fluid components are monitored. In the post-combustion phase, data are analyzed to determine properties such as combustion front velocity, stoichiometry, reaction kinetics, and mass balance of residual fluids (Sarathi, 1999; Moore et al., 2002; Gutierrez et al., 2012). A notable limitation prevalent in the majority of published ISC laboratory studies is the use of homogenized crushed rock samples loaded into the combustion reactors and tubes. While this approach facilitates experimental convenience and supports mineral reactivity, it raises critical questions about the fidelity of the observed combustion dynamics (Barzin et al., 2010; Zhu et al., 2021; Bazargan et al., 2011). Specifically, how combustion front and relevant reactions would evolve if the samples retained their natural properties, such as porosity, permeability, wettability, and the distribution of mineral inclusions.

In carbonate sedimentary rocks, known for their thermal instability, the primary minerals—calcite and dolomite—exhibit pronounced reactivity at elevated temperatures (Becattini et al., 2017). However, the recent studies (Ariskina et al., 2021) demonstrate that irrespective of rock and oil composition, both calcite and dolomite can contribute to a stable combustion front. This is facilitated by intensive coke formation and ease of combustion, leading

to inevitable CO<sub>2</sub> production that correlates directly with rock dissociation. Other studies (Pope et al., 2020) investigate the nature of the interaction between the components of crude oil and carbonate materials (calcite and dolomite) using thermogravimetric analysis (TGA). The activation temperatures of these minerals can affect the behavior of combustion dynamics. Dolomite reduces the heat release of the original bitumen due to the high activation energy, and calcite releases more heat for combustion. In addition to calcite and dolomite, clays may also be present in carbonates. It is reported that clays can act as a catalyst, which increase the efficiency of combustion (Kozlowski et al., 2015). Effects of clay mineral content (montmorillonite, kaolinite, chlorite and illite) in the formation have been studied by Li et al. (2021) and Ismail and Hascakir (2017), where it was found that they accelerate the formation of coke.

The changes that occur in carbonates at elevated temperatures can be conditionally divided into two groups: 1) changes in porosity and pore size distribution and 2) transformation of the mineral matrix and the formation of new minerals (Karunadasa et al., 2019). Changes in porosity can be expressed both in the formation of microcracks as a result of thermal expansion, and as a result of structural changes in the rock matrix. Heating the rock to temperatures above 150 °C can cause considerable destruction, increasing effective porosities due to calcite dilation (Yavuz et al., 2010). Carbonate rocks exhibit thermal expansion, which can lead to internal stress concentrations and cracking, particularly between and within grains. This is influenced by the random orientation of calcite crystals (Yavuz et al., 2010). In the work by Kalia and Balakotaiah (2009), samples of calcite and dolomite in cemented sandstone were studied. The study demonstrates that heating to 900 °C induces mineralogical changes, resulting in a 20% increase in porosity. Carbonate rocks, primarily composed of calcite (CaCO<sub>3</sub>) and dolomite (CaMg(CO<sub>3</sub>)<sub>2</sub>), undergo thermal decomposition when exposed to high temperatures. The dissolution of carbonate rocks is significantly influenced by temperature, flow rate, and dynamic water pressure conditions. Studies have shown that carbonate rock dissolution is more pronounced under normal and medium temperature conditions compared to low and high temperatures (Meng et al., 2022). The decomposition of these minerals can occur at relatively low temperatures (400-600 °C), affecting the bonding between the minerals and altering the rock's chemical stability (Sygała et al., 2013). Calcite primarily decomposes into calcium oxide (CaO) and carbon dioxide (CO2) when subjected to high temperatures. The decomposition of calcite begins at a slow rate around 700 °C and rapidly occurs beyond this temperature (Karunadasa et al., 2019). Dolomite decomposes in a more complex manner due to its dual composition of calcium and magnesium carbonates. The thermal decomposition of dolomite under nonisothermal conditions occurs at heating rates ranging from 2.5° to 15° per minute, starting at temperatures around 650 °C (923 K) and can last for several hours (Olszak-Humienik and Jablonski, 2015). The decomposition process results in the formation of calcium and magnesium oxides (CaO and MgO) and CO2. The kinetics of dolomite decomposition are influenced by factors such as temperature, heating rate, and the presence of CO<sub>2</sub>, which can affect the reactivity and stability of the resulting oxides (Valverde et al., 2015).

With a limited number of literatures focusing on mineralogical transformations during *in-situ* combustion, understanding these changes is vital for accurately characterizing variations in total porosity, pore connectivity, and pore size distribution—parameters that are essential for numerical modeling and field-scale applications of thermal EOR techniques. For instance, the formation of CaO and MgO can alter the rock's porosity and reactivity, potentially enhancing oil recovery by improving fluid flow pathways. The reactivity of CaO produced from dolomite decomposition makes it a

candidate for capturing  $CO_2$  as proposed by the Calcium-Looping (CaL) method (Valverde et al., 2015).

According to Alexander et al. (1962), Dabbous and Fulton (1974), Berna et al. (2013), pore surface area is tightly related to rocks porosity and permeability. In ISC context, knowing the extent of alteration of these parameters will dictate the efficiency of the combustion process. To this end, Aleksandrov and Hascakir (2015) utilized computed tomography, to examine the change of reservoir porosity and permeability during the ISC tests and identified the ideal values of initial oil saturation. In our previous studies, we examined the behavior of shale (Mukhametdinova et al., 2020) and dolomite-rich rocks (Mukhametdinova et al., 2022) observing the significant change of reservoir properties such as increase in porosity, permeability, shift of pore size distribution as well as the changes in mineral composition of rock exposed to the high-temperature combustion.

In this study, we aim to address critical gaps in understanding the petrophysical and lithological evolution of carbonate reservoirs subjected to laboratory modeling of in-situ combustion. The work is particularly significant for its use of consolidated rock samples, offering a more authentic representation of natural reservoir conditions, as opposed to the homogenized, crushed core models commonly used in the literature. By characterizing changes in reservoir porosity, pore size distribution, and mineral transformations, we offer critical insights into the interplay of thermal, chemical, and mechanical processes. These insights also have implications for the utilization of thermally treated reservoirs in the post-production phase. Although the study focuses on the chemical and physical effects of combustion on the rock, these findings are fundamentally important for understanding how petrophysical alterations—such as the shift of the rock to the strong water-wet state and increased microporosity post-combustion-shed light on options for repurposing the reservoirs after thermal EOR, including for CO<sub>2</sub> storage (Raza et al., 2017; Alanazi et al., 2023; Fathy et al., 2023).

#### 2. Materials

The investigated carbonate samples are attributed to Vereysk Formation, which is deposited within Volga-Ural Petroleum Basin during Moscovian Stage ( $C_2$ m) (Fig. 1). The target oilfield is primarily composed of limestone lithofacies, including packstone, grainstone, and boundstone, with intermittent interbeds of argillites, siltstones, and sandstones in the upper stratigraphy. Classified as a heavy oil reservoir, the core sample utilized in our combustion experiment exhibited an average porosity of 14%, a gas permeability of 35 millidarcies, and an oil density ranging between 0.904 and 0.942 g/cm<sup>3</sup>.

In total, 18 core plugs were used to construct a consolidated core model that was loaded into the reactor. The locations of samples inside the tube, their separation by zones, and corresponding maximal combustion temperatures are detailed in Table 1. For additional tests, the duplicate core fragments of target oilfield were used to study the initial properties of the rock before combustion.

#### 3. Methods

#### 3.1. Experimental workflow

The combustion tube experiment on the consolidated core was performed using medium-pressure combustion tube (MPCT, HotTec, Calgary) equipment. The MPCT experiment was conducted on a custom-made tube with a length of 710 mm, and an inner diameter of 53 mm. The detailed description of the tube installation is presented in Popov et al. (2021) and Askarova et al. (2022) while

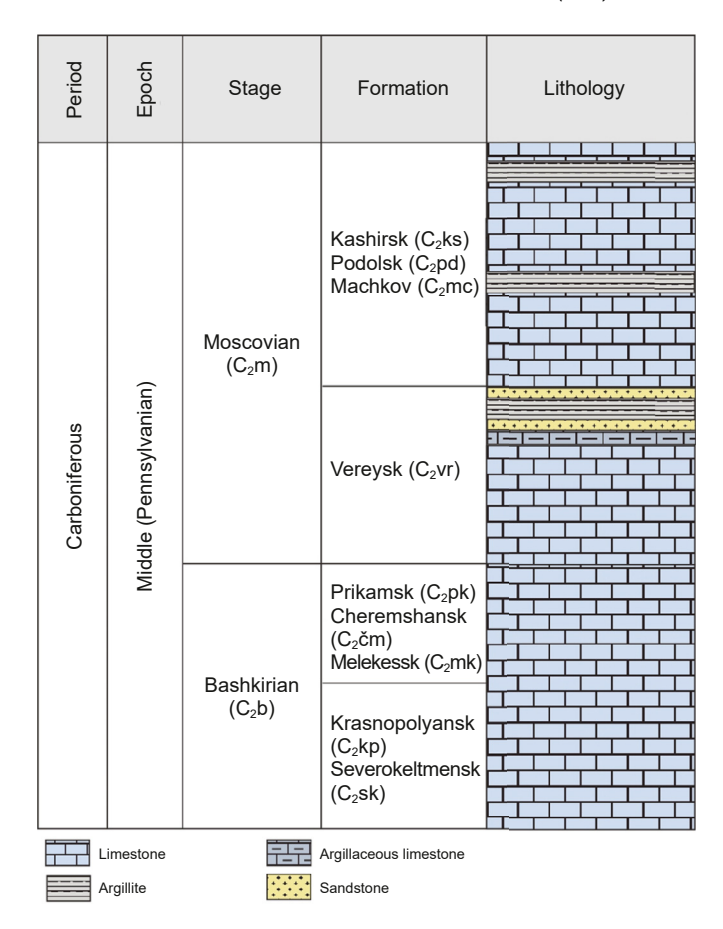


Fig. 1. Target formation in the regional stratigraphic chart area.

the preparation of the core model and cementing in the steel sleeve are described in Askarova et al. (2020). The consolidated core model in the experiment consisted of 18 core plugs from the target formation (Table 2). The pressure was equal to 12.4 MPa, and the initial temperature was 33 °C. The consequent displacement of the brine created the initial water and oil saturation by dead oil. The combustion tube was on adiabatic control, and the wall temperatures were set to track the core model temperatures with a 5 °C lag to minimize heat losses.

To obtain the above-mentioned value of initial oil saturation in experiment, pretreatment stages (cold and hot water injection stages) were performed, and favorable conditions for the combustion process were achieved. The stages of the combustion test included water injection at 125 °C, water injection at 300 °C, air injection (at 90 m $^3$  (st)/m $^2$ /h vol. rate), ignition, helium purge, pressure and temperature relief.

Prior to the experimental modeling of the *in-situ* combustion, the set of core samples (plugs and samples of irregular shape) underwent a workflow aimed at defining the initial petrophysical and lithological properties (Fig. 2). The entire core collection consisted of cylinder plugs and core fragments of irregular shape. The measurements were repeated on the same core samples (except for the tomography on drilled mini plugs) before and after the thermal exposure. The porosity was investigated by means of gas porosimetry, NMR, and gravimetric measurements (liquid saturation porosity) while the microcomputed X-ray tomography and NMR characterized the pore size distribution. Optical microscopy, scanning electron microscopy, and X-ray diffraction registered the changes in the rock composition and microstructure pre- and post combustion. Additionally, drop shape analysis and low-

**Table 1**List of rock samples.

Sample ID	Zone of the tube	Location in the combustion tube from inlet, mm	Exposure temperature, °C
15	1	18.54	397
20		45.08	397
16-2		73.27	397
18-1		117.86	481
19-2		165.36	481
12	2	208.44	468
23		251.80	468
20-1		293.58	440
18-2		332.66	440
22-3	3	365.24	411
24-2		390.98	411
22-1		425.95	401
19-1		466.55	401
20-2		507.67	438
25	4	553.29	438
21		600.35	424
11-2		649.75	424
22-2		691.74	307

**Table 2**Parameters of the core model used in the MPCT experiment.

Parameter	Value
Length, mm	710
Diameter, mm	53
Porosity by gas, %	15
Permeability by gas, mD	10.9
Oil saturation at ignition, %	25

temperature nitrogen adsorption were used to study the wettability and specific surface area of the collection, respectively.

#### 3.2. NMR relaxometry and gravimetric porosity

Low-field nuclear magnetic resonance (LF-NMR) relaxometry is an analytical technique employed for saturation, and porosity assessment, evaluation of viscosity, wettability, permeability, and notably, the characterization of pore size distribution within reservoir rocks (Straley et al., 1997; Markovic et al., 2022). In this study, we use LF-NMR measurements to assess alterations in the porosity and pore size distribution of rocks prior to and subsequent to their exposure to combustion. The NMR setup is a laboratory analyzer of core samples operating at the 2-MHz frequency with a magnetic field of 0.05 T. The  $\rm T_2$  relaxation measurements resulted from the Carr-Purcell-Meiboom-Gill pulse sequence with the time-echo (TE =  $\rm 2\tau$ ) set to 0.1 ms. Preliminary tests justified the number

of trains (accumulations) of the applied pulse sequence ( $90^{\circ}$ – $\tau$ - $180^{\circ}$ – $2\tau$ – $180^{\circ}$ – $\dots$ – $n\tau$ - $180^{\circ}$ ); the signal-to-noise ratio was equal to or above 100. Samples were analyzed in 100% water-saturated state before and post combustion. The obtained data was processed using GIT Systems Advanced v.7.5.1 software (Green Imaging Technologies) (GIT, 2014). The gravimetric or liquid saturation (LS) porosity resulted from gravimetric measurements of core plugs' mass and volume in dried and water-saturated states and calculation of the open porosity for each individual sample.

#### 3.3. X-ray computed tomography (µCT)

The X-ray computed micro-tomography analysis was performed to analyze the changes of porous space and rock matrix after the *insitu* combustion process in terms of absolute changes of 3D image of the core model as well as pore size distribution of the selected areas. The GE Phoenix v|tome|x L 240/180 industrial dual tube X-Ray tomography system was used for scanning full core model in a sealed stainless steel pipe and drilled mini cores in a cone beam mode at 100–160 kV accelerating voltage. The geometrical resolution was 30  $\mu$ m/voxel for full Ø50 mm core in a steel pipe and 5  $\mu$ m/voxel for Ø8 mm mini-core, respectively. The X-Ray 3D microtomography images were processed using FEI PerGeos 1.5 software for images registered before and after combustion as well as for void/mineral skeleton segmentation (PerGeos, 2018). The GeoDict 2022 software was used for total, open, closed porosity and pore size distribution analysis.

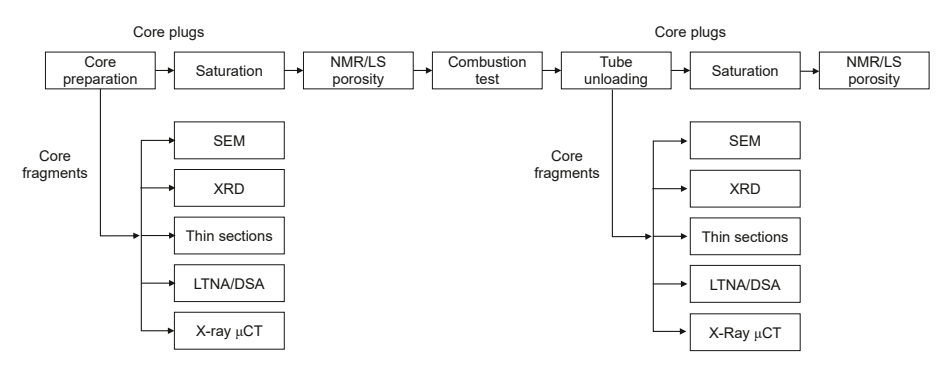


Fig. 2. The workflow of core samples investigation.

## 3.4. Scanning electron microscopy (SEM), X-ray diffraction (XRD) and optical petrography

Scanning electron microscopy was utilized for detailed microstructural investigation of rock samples before and after the thermal exposure. The Thermo Fisher Scientific Ouattro S machine allows to analyze small 5 mm size rock probes, splited from the cylindrical sample. The electron beam current ranges from 1 pA to 200 nA, the accelerating voltage is increased 200 V to 30 kV. In current study, we used both secondary and backscattered modes during the scanning at accelerating voltage of 10-15 kV (Erdman and Drenzek, 2013). The highest scanning quality (spatial resolution) was 5 nm, and the resulting images were 1536  $\times$  1094 px in size. An integrated EDX (energy-dispersive X-Ray spectrometer by Quantax, Bruker, USA) was used for semiguantitative analysis of chemical element composition. Lithotyping, structure and void space analysis of thin sections were performed the petrographic ZEISS AxioScope 5 microscope according to the principles of Dunham classification (Dunham and Ham, 1962). The XRD analysis provided a semi-quantitative determination of rock sample mineralogy. Mineralogy analysis on core powder was performed using the benchtop DRON-3 (produced by Burevestnik JSC) X-Ray diffractometer unit.

#### 3.5. Low-temperature nitrogen adsorption (LTNA)

Specific surface area was measured by Sorbi-MS device (Meta MS), which is designed for providing specific surface area and porosity information, including external surface area, mesopore volume, and pore size distribution in materials science research and quality control in high-tech industries. The Sorbi-MS is equipped with certified calibration samples of dispersed porous materials with known specific surface area. The Brunauer-Emmett-Teller (BET) theory was used to calculate the specific surface area of the rock samples. Nitrogen was used as a gas.

#### 3.6. Rock wettability by drop shape analysis (DSA)

Conventionally, rock wettability is determined by the Amott-Harvey, U.S. Bureau of Mines (USBM), and contact angle techniques (Yekeen et al., 2020). Contact angle measurements, used in this study, are universally recognized method, used for solid-gasliquid systems, and for assessing wettability alterations driven by variations in temperature, pressure, and brine chemistry (McPhee et al., 2015).

Kruss DSA 30s drop shape analyzer was used. Data acquisition and analysis were streamlined through its Kruss Advance software. The contact angle between a wetting phase and a substrate was measured via the sessile droplet method. Droplet of deionized water was placed on the solid surface and imaged with a high-speed camera. Image recognition algorithm discerns the droplet's profile and its interface with the substrate, compared against theoretical contours derived from the Young-Laplace equation, given by Eq. (1):

$$\cos(\theta) = \frac{\sigma_{SG} - \sigma_{SL}}{\sigma_{LG}} \tag{1}$$

where  $\sigma_{SG}$  represents the solid-gas;  $\sigma_{SL}$  solid-liquid; and  $\sigma_{LG}$  liquid-gas surface tensions, respectively. Samples were smoothed using sandpaper with grit size P500 to achieve a consistent surface texture. Each sample was blow-dried with compressed nitrogen before measurements to remove dust particles. Each droplet was recorded for 5 s, with images captured at 20-ms intervals. This procedure was reiterated across different sample sections, for a

minimum of five droplets providing at least 25 contact angle data points. Final contact angle of the sample was taken as a mean value of all contact angles measured on the sample.

#### 3.7. Core preparation

The core saturation procedure consisted of vacuuming the samples, capillary imbibition, and injection of a saturating fluid (distilled water) under a pressure of 15 MPa using an automatic saturating unit Geologika PIK-SK. Solvent cleaning (extraction) consisted of cleaning the rock samples (core plugs and fragments) with chloroform. After extraction, the rock samples were dried at a temperature of 105 °C in the laboratory-heating oven Memmert VO400 until the constant weight ( $\Delta$ 0.001 g).

#### 4. Results

## 4.1. Characterization of the rock microstructure before and after the exposure

Section 4.1 reports qualitative changes registered for core samples before and after the combustion. Initial analysis is performed by optical microscopy of thin sections and X-ray diffraction to define the mineral composition of the rock under study. The core plugs are examined by X-ray tomography at 30  $\mu$ m/voxel resolution for preliminary evaluation of the pore structure alteration. The core fragments are investigated by scanning electron microscopy to track the microstructural and morphology changes in the rock.

#### 4.1.1. Mineral matrix by optical microscopy and XRD

Petrographic analysis characterized the rock as grainstone according to the Dunham classification (Dunham and Ham, 1962). The rock is composed of calcite shells and shell fragments, the size of fragments varies in the range of  $100-500~\mu m$  (Fig. 3). The interparticle pores are observed, and the porosity is approximately 10%-15%. The samples #20-1 and #22-2 are characterized by large individual dissolution pores with the size of  $50-200~\mu m$ . The average pore size ranges from  $10~to~150~\mu m$ . However, the analysis of thin sections after the combustion did not provide comprehensive information on occurred changes in the rock microstructure at the scale of optical microscopy (Appendix A, Fig. 17).

The composition of rock samples includes a variety of rock-forming minerals (Table 3). The initial XRD analysis showed that most of the samples are composed of calcite (>95%) with minor amount of quartz and clay minerals. The XRD of rock after the combustion show that the amount of dolomite systematically decreased in all the samples with the dolomite present in their initial state (Table 4). The samples #12, #20-1, #22-1, and #22-3 contain anhydrite after the experiment up to 3.2%.

#### 4.1.2. Porosity by μCT on Ø50 mm core plugs

The X-Ray  $\mu$ CT images of initial samples ( $\emptyset$ 50 mm) (Appendix A, Fig. 18) show that the morphology of rock varies depending on amount of the dense carbonate, as well as pore sizes and homogeneity of pore space distribution. Samples #16-2 and #25 contain fractures; the pore sizes are below the spatial resolution resulting to the regions of sub- or non-resolved pores marked as regions with lower X-ray density (darker spots) on the slices in comparison to dense carbonate parts. This provides a limitation to porosity measurement to the pores below 50  $\mu$ m.

However, the differential images, illustrating changes in porous space or mineral skeleton for selected sample (#25) are presented in Fig. 4. Observed changed areas are highlighted with brighter tones. The differential picture of registered 3D images shows minimal changes in a porous structure with a low intensity noise-

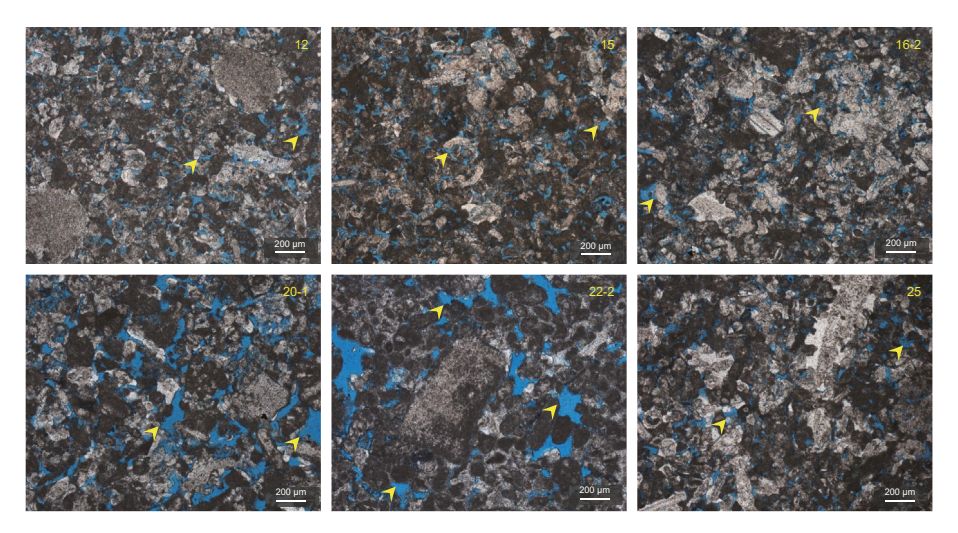


Fig. 3. Microphotographs of investigated grainstone, the rock is composed of numerous calcite shell fragments. Arrows indicate the pores; pores are highlighted by blue colour. Samples #20-1 and #22-2 are characterized by dissolution-caused large pores, other samples have intergranular porosity.

**Table 3**Mineral composition of rock samples before the combustion experiment.

Sample ID	Mineral composition, wt%				
	Quartz	Calcite	Dolomite	Clay total	
11-2	0.9	98.1	1	0	
12	0.5	96.6	1.5	1.4	
15	0.5	99.5	0	0	
16-2	1.1	98.2	0.7	0	
18-1	0.5	99.5	0	0	
18-2	0.8	99.2	0	0	
19-1	0.9	96.6	2.5	0	
19-2	0.5	88.6	10.9	0	
20-1	0.5	90.6	8.9	0	
20-2	0.8	94.4	4.8	0	
21	0.8	92.1	7.1	0	
22-1	1.7	95.9	2.4	0	
22-2	0.7	98.2	1.1	0	
22-3	0.7	96.2	3.1	0	
23	0.8	97.5	0.9	0.8	
24-2	0.5	95.7	3.8	0	
25	0.5	97.9	1.6	0	
Minimum	0.5	88.6	0	0	
Maximum	1.70	99.50	10.90	1.40	
Average	0.75	96.16	2.96	0.13	

like pattern. Some difference in larger pores is related to the residual fluid content. Highlighted parts are related to dense inclusion locations and may be caused by chemical reactions and mineral transformations. The most significant changes can be explained by fractures closed after the combustion (samples #16-2 and #25) and reopened after the fluid extraction, and mechanically damaged parts of the sample.

These damaged parts contribute to the porosity change — decreased porosity for samples #16-2 and #25, while other samples demonstrate negligible changes in relative pore size distribution before and after the combustion (before extraction) at given resolution (Fig. 5). The total porosity calculated from X-ray  $\mu\text{CT}$  segmented images (Table 5) is noticeable lower to one measured by other techniques due to the low resolution (30  $\mu\text{m/voxel})$  on large core samples since the information on pores less than 50  $\mu\text{m}$  is excluded. Therefore, technically, we do not observe the connectivity in 3D porous structure, and the most porosity is formed due to the pores of first bin on histogram (Table 5).

To summarize, the preliminary tomography on full Ø50 mm

samples demonstrated that the obtained total porosity is low and has no connectivity, and the average measured porosity gain is related to the mechanical changes. The resolution of 30  $\mu m/voxel$  with segmentation of void space is not effective for identification of porosity change for the samples after treatment. Similarly, comparing grayscale images primarily enables the identification of closed fractures and mineral alterations in dense inclusions, but does not discern the changes in the primary porosity of the rock matrix. Therefore, most of the pores are below 45  $\mu m$  that can be resolved by tomography of Ø8 mm mini cores at geometrical resolution of 5  $\mu m/voxel$ . Therefore, the workflow of the X-ray tomography analysis was modified accordingly, and the additional measurements on drilled mini cores were implemented.

## 4.1.3. Pore nanostructure alteration by scanning electron microscopy

The combined analysis by SEM and energy-dispersive X-ray spectroscopy revealed significant alterations at micro- and nanometer scale in porous space structure and mineral matrix in post combustion samples. Fig. 6 demonstrates typical initial micro-structure of the carbonate samples in their initial state before combustion. The surface of the calcite crystals is smooth and clear without any other phases.

The most evidential alteration of mineral matrix is roughing of calcite minerals: microstructure of the crystals after the experiment became rough and porous (Fig. 7(c), (e), (f), (g), (i), and (j)). This effect is common for most of the analyzed samples. Coarsening of crystals is associated with the calcite decomposition and formation of calcium oxide on the surface of the original crystals, as demonstrated by XRD results. The pores are located within the carbonate grains and have the size less than 1  $\mu$ m. The second alteration is the cavity formation characterized by numerous dissolution traces (Fig. 7(a)). In few samples, microfractures were observed (Fig. 7(e), (d)): fractures are local and occur sporadically on crystals, in length and width up to 50  $\mu$ m and 0.5  $\mu$ m, respectively. The third alteration is formation of new phases: Fig. 7(c), (f) demonstrate newly formed crystals of fluorite (CaF<sub>2</sub>), which fill the pore space, and this effect is observed for all samples. Additional EDX analysis results (Fig. 9(b) and (c)) show coexisting of Ca and F within same crystals (weight of Ca and F are 1:2), and that confirms presence of CaF<sub>2</sub> in the rock samples after combustion. Fig. 7(k) shows individual crystals of anhydrite in the porous space. Fig. 8(a) shows the example of calcite crystal decomposition with the formation of CaO, the effect is rare

**Table 4**Mineral composition of rock samples after the combustion experiment.

Sample ID	Mineral composition, wt%	Mineral composition, wt%							
	Combustion temperature, °C	Quartz	Calcite	Dolomite	Clay total	Anhydrite			
11-2	424	0.8	98.6	0	0	0.6			
12	468	0	98.9	0	1.1	0			
15	397	0.7	99.3	0	0	0			
16-2	397	1.4	98.6	0	0	0			
18-1	481	0.9	99.1	0	0	0			
18-2	440	0.5	98.0	0	1.5	0			
19-1	401	1.6	98.4	0	0	0			
19-2	481	0.8	92.4	6.2	0.6	0			
20-1	440	1.2	93.0	5.0	0	0.8			
20-2	438	1.0	95.3	3.7	0	0			
21	424	1.0	96.0	3.0	0	0			
22-1	401	0.5	94.4	1.9	0	3.2			
22-2	307	2.0	96.0	2.0	0	0			
22-3	411	1.3	96.9	1.1	0	0.7			
23	468	0.8	98.2	1.0	0	0			
24-2	411	1.2	98.8	0	0	0			
25	438	2.6	96.6	0.8	0	0			
Minimum		0	92.4	0	0	0			
Maximum		2.6	99.3	6.2	1.5	3.2			
Average		1.1	96.9	1.5	0.2	0.3			

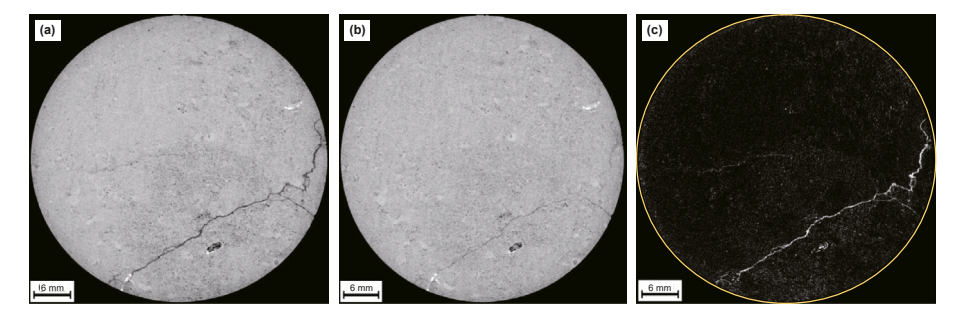


Fig. 4. Slices of 3D X-Ray μCT images for sample #25 before (a) and after (b) combustion; (c) Differential picture of slice after the combustion compared to initial one.

and observed locally. EDX analysis of the same area demonstrates the presence of Ca and O (atom weight is 1:1), which confirms that the calcite was decomposed into calcium oxide.

## 4.2. Reservoir rock properties: porosity, pore size, wettability and specific surface

Current section introduces the quantitative tools used for porosity and porous space evaluation. X-ray tomography at high resolution shows enhanced results on rock pore geometry in addition to the previously obtained information. NMR provides an accurate data on rock porosity and pore size alteration. Contact angle measurements reflect the alteration in rock wettability while the LNTA method demonstrates the change in specific surface.

## 4.2.1. Porosity by NMR/LS and pore size distribution based on $T_2$ relaxation

Porosity was quantified from two independent methods—NMR relaxometry and mass-volume measurements of the fully-saturated core plugs (initial state) and samples after the combustion. NMR tests were combined with the measurements of the mass of each sample before and after the saturation with water. These values are indicted as porosity by liquid saturation (LS). Initial porosity by LS for samples ranged from 11.9% to 20.2% with an average value of 14.8% (Fig. 10), while the NMR analysis showed the range from 7.8% to 23.1%, with an average value of 16.6%. Both methods showed increased values of porosity for samples after the

combustion.

These results support the hypothesis about thermal decomposition of calcite and dolomite and other observed changes registered by SEM and X-ray CT (Figs. 5 and 7). Currently, the noted increase in porosity is mostly contributed by the small newlyformed pores and altered porous space structure including changes in the rock microtexture.

The pore size distribution was estimated based on the  $T_2$  spectra for saturated  $\emptyset$ 50 mm samples before combustion and after the final extraction stage. The recalculation of the  $T_2$  pore radius is performed using the surface relaxivity coefficient equal to  $10~\mu\text{m}/\text{ms}$ . Fig. 11 depicts the distributions for three selected samples: #12, #15 and #20-1. As shown in Fig. 11, a shift of the  $T_2$  logarithmic mean value ( $T_{2\text{lm}}$ ) is a result of formation of smaller pores caused by thermal decomposition of minerals, which corresponds to increase in a specific surface that will be discussed later. In all three cases, most newly-formed pores are registered in the range from 1 to  $T_2$ 0 mm (pore radius). Some pores are located in the range from 0.1 to  $T_2$ 1 mm, which indicates the alteration in the mineral matrix of the rock.

#### 4.2.2. Porosity and pore size by $\mu$ CT on Ø8 mm core plugs

Analysis of mini core samples (Fig. 12) at 5  $\mu$ m/voxel resolution provides insights into porosity and pore geometry alteration at 10–45  $\mu$ m scale (Appendix A, Fig. 19). The values of porosity for 5  $\mu$ m/voxel scan fall in the range of 13%–18% (in comparison to 1%–8% registered at 30  $\mu$ m/voxel resolution), and most pores are

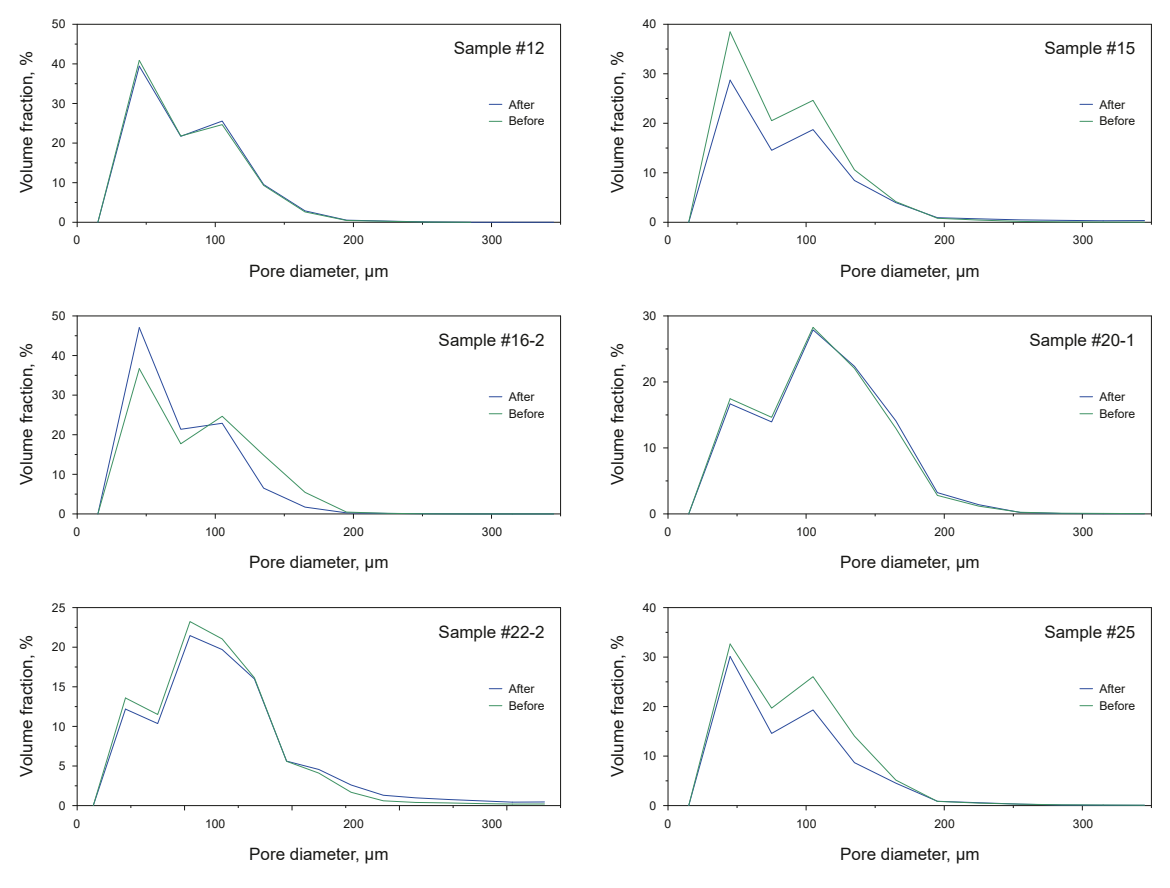


Fig. 5. Relative pore size distribution for Ø50 mm samples before (green) and after combustion (blue) by μCT with resolution of 30 μm/voxel.

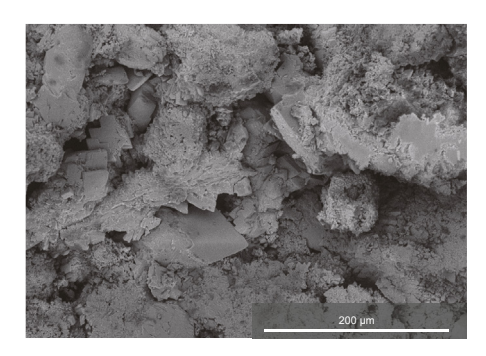
**Table 5** Porosity of samples ( $\emptyset$ 50 mm) before and after the combustion and after fluids extraction based on X-ray  $\mu$ CT with 30  $\mu$ m/voxel size.

Sample ID	12	15	16-2	20-1	22-2	25
State	Total	porosity,	%			
Before combustion After combustion After extraction	2.8 3.5 1.7	1.3 1.5 2.5	6.6 3.2 2.8	6.4 7.7 7.6	6.9 6.9 7.7	5.4 4.9 2.0

characterized as open and connected (Table 6).

The analysis of mini-cores at 5  $\mu m/voxel$  resolution is more informative, yet is limited in the analysis of the same slice or area of the sample since the post combustion Ø8 mm plugs were drilled out from Ø50 mm samples. As pre combustion models (initial

samples), the new set of duplicate Ø8 mm samples were prepared from areas next to main Ø50 mm cores. Taking into account the significant heterogeneity of the rock, analysis of combustioncaused alteration cannot be performed for the same area of the rock (as previously done for large core plugs in Section 4.1.2). However, comparison of duplicate Ø8 mm samples before and after the exposure shows the similar pore size distribution (Fig. 12) and general morphology (Appendix A, Fig. 19). The variability of the porosity and pore size distribution for different areas of the same Ø50 mm sample #22-2 after the combustion is illustrated for three sub-samples (Fig. 12, Table 6). Despite the fact that analysis of samples from different areas before and after combustion is complicated by the associated variability in the porosity and pore size of inhomogeneous samples, the overall structure at 5 μm/voxel remains unchanged. Tomography does not reveal a transformation of individual carbonate rock grains and changes in the structure of



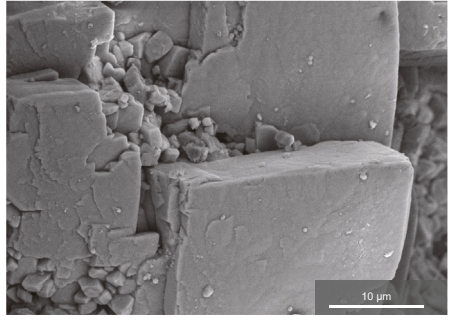
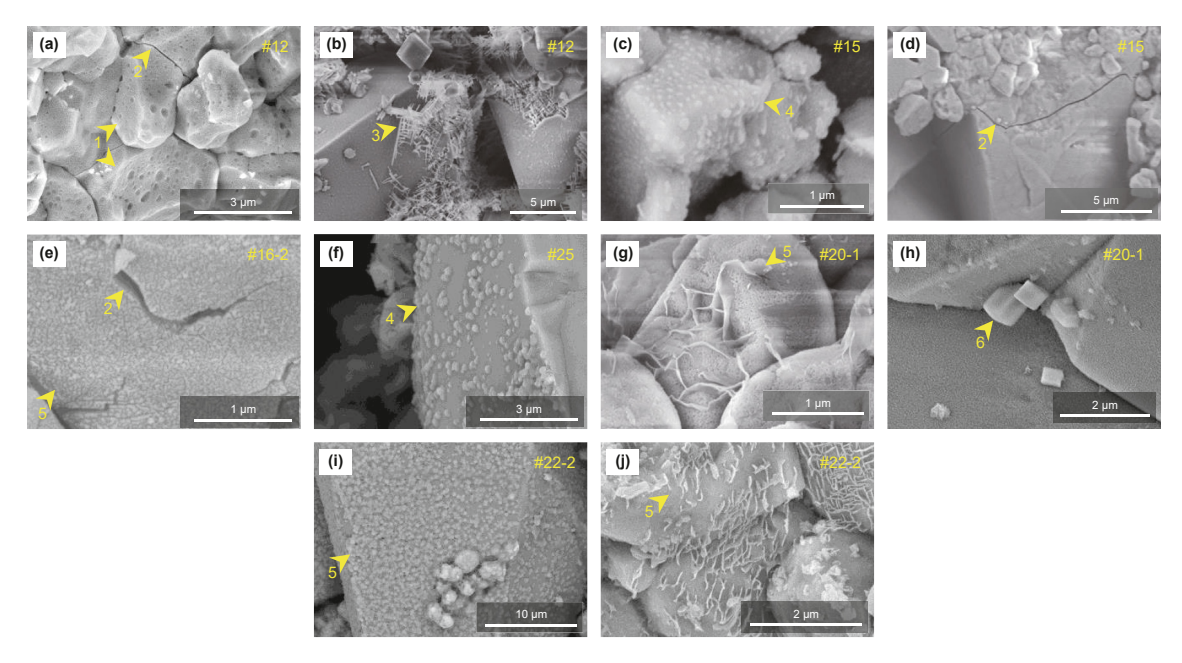


Fig. 6. Initial typical microstructure of the sample #12.



**Fig. 7.** Alterations of rock samples after the combustion: 1—traces of dissolution, 2—microfractures within grains, 3—formation of new crystals of CaO, 4—aggregates of CaF<sub>2</sub>, 5—rough surface of the calcite crystals, 6—new crystals of anhydrite.

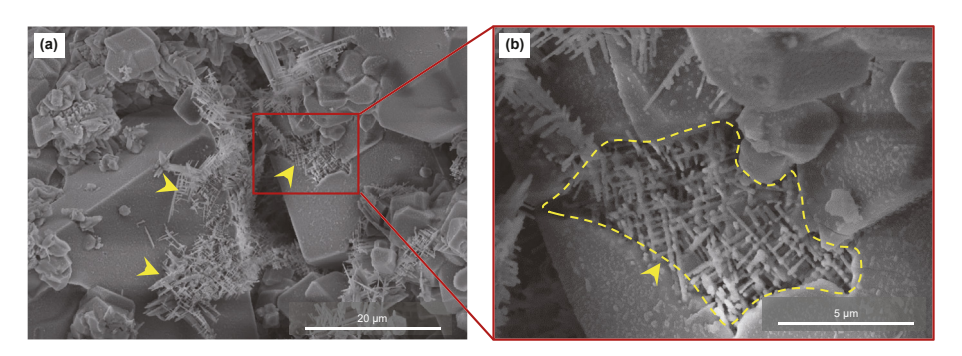


Fig. 8. Alterations of mineral matrix in carbonate rock samples after combustion. (a) Newly formed crystals in the pore space with the dominance of calcium and fluorite; (b) Decomposition of calcite crystals, the crystal is filled by calcium oxide.

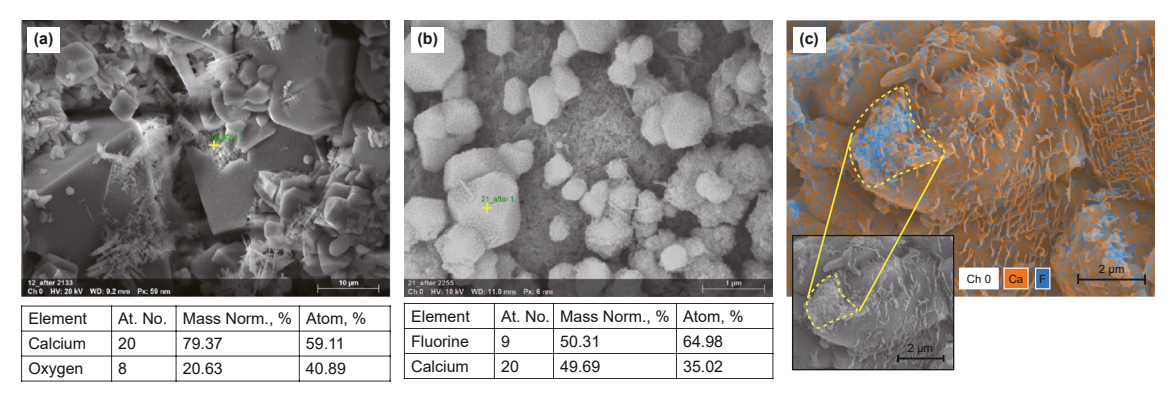
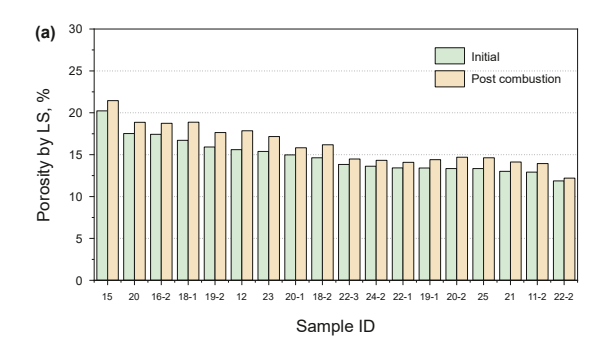


Fig. 9. EDX elemental analysis of newly formed crystals. (a) Sample #12, point analysis demonstrates the presence of Ca and O in decomposed calcite; (b) Sample #21, crystals are composed of Ca and F; (c) Sample #22-2, EDX elemental mapping shows coexisting of Ca and F within one local area.

the porous space. Thus, main changes in the void space observed by other techniques occur on a scale less than 5  $\mu m$ .

4.2.3. Specific surface and wettability alteration
Results of the BET analysis (low-temperature nitrogen

adsorption) demonstrated the changes in the specific surface area for investigated samples (Fig. 13). We have selected three samples located in different temperature zones of the combustion tube and repeated the measurements on probes of 1 g before and after the combustion experiment. The initial values varied around



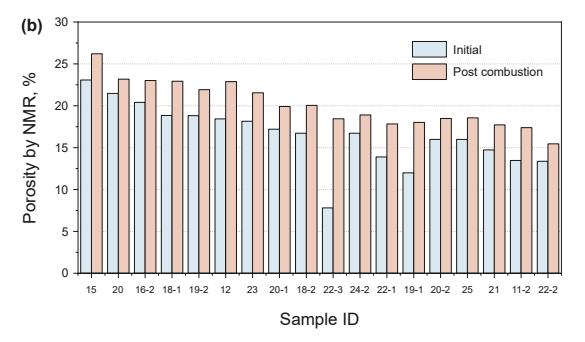
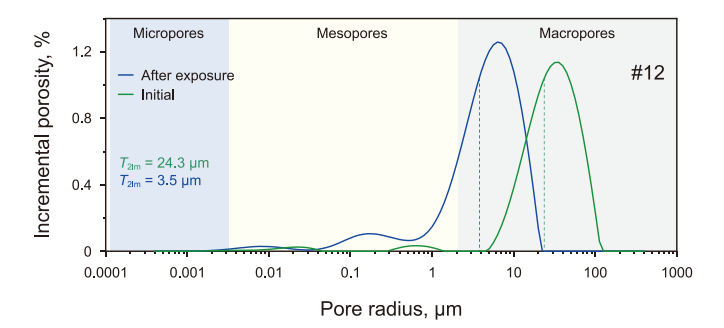
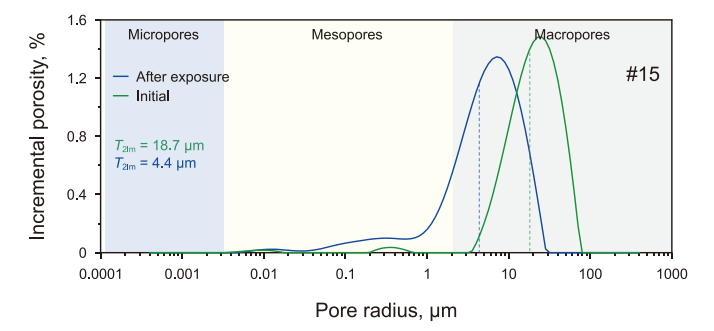
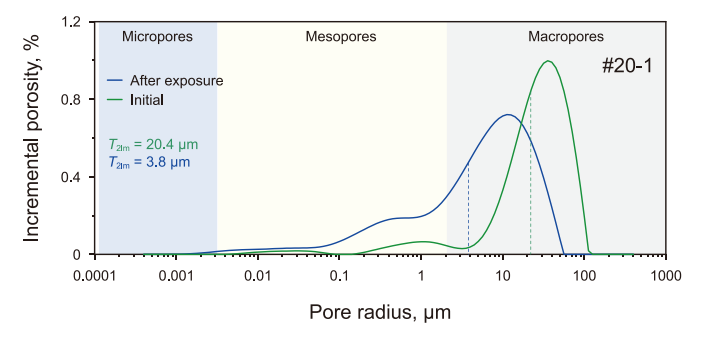


Fig. 10. Porosity by LS (a) and NMR (b) for samples before and after combustion.







 $\textbf{Fig. 11.} \ \ \text{Pore size distribution by NMR for samples before and after combustion.}$ 

 $0.2-0.3~{\rm m}^2/{\rm g}$ , and, as expected, we observed increased numbers in post combustion samples. Final values fell into  $0.7-1.0~{\rm m}^2/{\rm g}$  range, which indicates more than double increase of the surface area. It is explained by transformed porous space and mineral decomposition of the calcite and dolomite.

Reservoir wettability is predominantly determined by oil-brine-rock interactions. Typically, reservoirs are water-saturated before oil migration, and the rock's water-wet nature results in a thin aqueous layer on its surface. The wettability of the sample based on the contact angle measurements can be classified according to Puntervold et al. (2023). From Fig. 14(a) it can be observed that the

target carbonate rock samples fall into the water-wet category in their initial state before combustion. This categorization is based on their contact angles, which range from  $44^\circ$  to  $69^\circ$ , with an average contact angle of  $52.5^\circ$ . Conversely, the contact angles of samples post combustion range from  $7^\circ$  to  $19^\circ$ , with an average of  $11.4^\circ$ , classifying them as strongly water-wet, as depicted in Fig. 14(b). A paired two-sample T-test was applied to quantify the differences in contact angle distributions before and after subjecting the samples to in-situ combustion. A p-value of  $8.8\times10^{-7}$  indicates a significant difference between the means of the two populations.

#### 5. Discussion

#### 5.1. Mineral matrix alterations caused by combustion

First part of the current research was focused on the mineral matrix alterations and formation of new minerals by number of techniques (optical microscopy, XRD and SEM). The summary of observed changes in post combustion samples is given in Fig. 15.

Petrographic analysis did not reveal significant changes in the rock, and it is explained by the technical limitations of the method. In turn, the XRD demonstrates complete dolomite decomposition as result of the thermal exposure and formation of anhydrite mineral, which is registered by XRD and SEM techniques. The samples #12, #20-1, #22-1, and #22-3 contain up to 3.2% of anhydrite after the combustion experiment. Anhydrite formation is a result of dolomite and calcite decomposition (source of Ca<sup>2+</sup> and Mg<sup>2+</sup> ions), while the sulfur can originate from organic matter in the rock. In addition, as result of the dolomite decomposition, the relative calcite fraction can increase for exposed samples. Small variations of a certain mineral content in samples can also be explained by microscale heterogeneities. We posit that CaO reacts with sulfur-containing compound (sulfur oxide or hydrogen sulfide) and form the anhydrite in presence of the water. Therefore, the sulfur originates from the organic matter since the rock mineral matrix does not contain sulfur-rich components. However, we did not detect any components containing Mg. SEM images demonstrate that new anhydrite crystals are originated in the pore space and partially fill it, however, due to their small amount and size, do not significantly affect the porosity and permeability.

Another mineral registered by SEM-EDX is a fluorite (CaF<sub>2</sub>), which was previously not detected by XRD due to its relatively small amount and small particle sizes. It is suggested that  $F^-$  ions originate from the cement used in core model packing, whereas  $Ca^{2+}$  result from two processes:  $CaCO_3$  dissolution and decomposition. Both ion groups were present in the brine used for flooding whereas all the  $CaF_2$  crystals are located exclusively in a porous space. Formation of fluorite  $CaF_2$  is directly associated with the fluorine-containing cement decomposition under high-temperature combustion.  $CaF_2$  crystals are 2  $\mu$ m size in average,

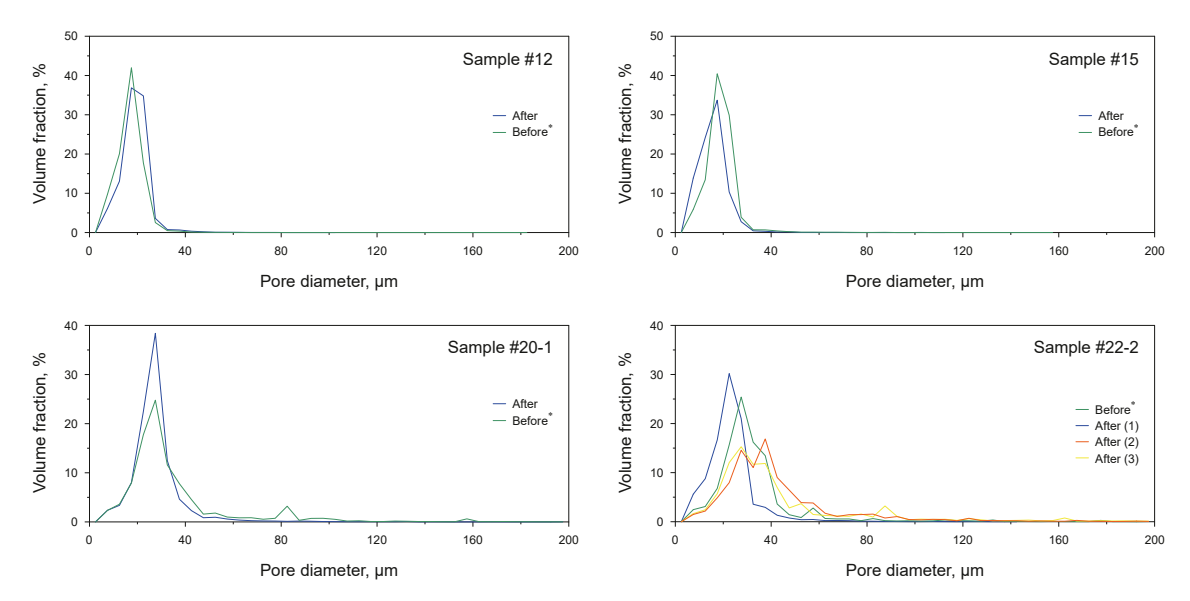


Fig. 12. Pore size distribution for Ø8 mm samples before (duplicate samples, in blue) and after combustion & extraction (green) based on X-ray μCT at 5 μm/voxel resolution.

**Table 6**Open and closed porosity for 8 mm mini-core samples before combustion and after combustion and following fluids extraction based on X-ray μCT with 5 μm/voxel resolution.

Sample ID	12	12		15		20-1		22-2	
Porosity, %	Open	Closed	Open	Closed	Open	Closed	Open	Closed	
Before test <sup>a</sup>	12.3	0.9	14.8	0.6	17.2	0.4	13.4	0.4	
After combustion and extraction	15.9	0.5	10.3	1.7	16.7	0.3	10.1	0.8	
							10.8	0.3	
							8.5	0.3	

<sup>&</sup>lt;sup>a</sup> Duplicate samples were used as 'pre combustion/initial samples'.

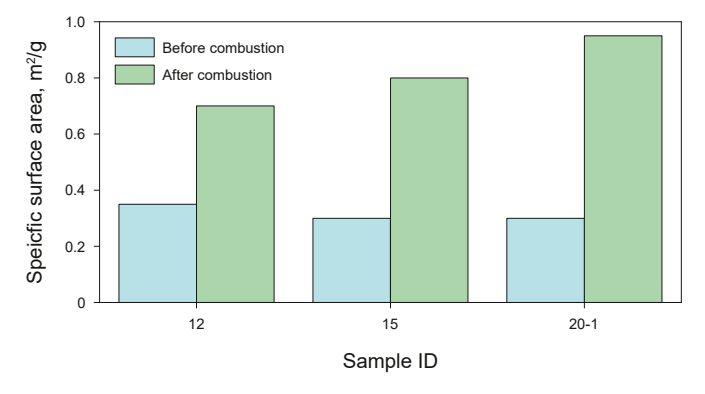


Fig. 13. Change of specific surface area of selected samples before and after ISC.

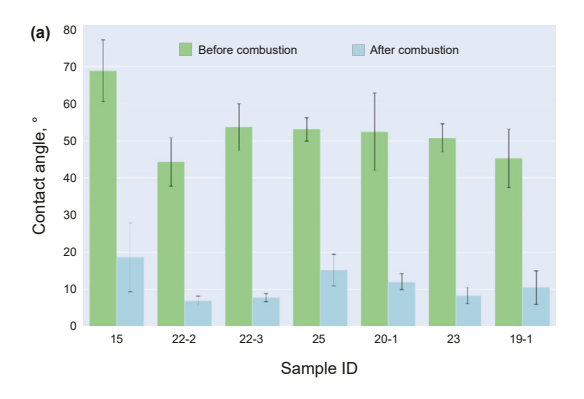
and occupy the microporous pores in the rock. Observed destruction of carbonate minerals already have been described in our previous studies of the laboratory modeling of *in-situ* combustion technology (Karamov et al., 2022; Mukhametdinova et al., 2022), where MgO crystals resulted from the dolomite decomposition and formed the dolomite aggregates. The anhydrite formation was also described in Karamov et al. (2022).

The key process of new minerals formation is the decomposition of carbonate mineral matrix, which supplies calcium. The chemical equations of the calcite  $(CaCO_3)$  and dolomite  $(CaMg(CO_3)_2)$  decomposition are shown below:

$$CaCO_3(s) \rightarrow CaO(s) + CO_2$$
 (2)

$$CaMg(CO_3)_2 \rightarrow CaCO_3 + MgO + CO_2 \rightarrow CaO + MgO + CO_2 \qquad (3)$$

The crystals of CaO were identified locally, and the process was described by Eq. (2) and by Eq. (3). The formation of CaO crystals result in damaging the initially smooth calcite crystals; the decomposition occurs only on the surface of the crystals. The crystal surface damage led to the increase in specific surface and complexity of the porous space structure. Our findings are consistent with the existing literature, which shows that calcite mainly decomposes into calcium oxide (CaO) and carbon dioxide (CO<sub>2</sub>) under high temperatures. The effect of calcite dissolution is observed for carbonate rock during contact with water under high pressure and temperature conditions (Larson and Emmons, 2021). The similar effects have also been reported by other research groups (Chen et al., 1998; Geng et al., 2017; Zheng et al., 2020). Temperature, flow rate, and dynamic water pressure conditions have a significant impact on the dissolution of carbonate rocks. The exposure temperature primarily influences the degree of calcite decomposition: for samples exposed to highest temperatures (for example, sample #12 at 468 °C), we observe pronounced alteration of calcite crystals with the formation of CaO, whereas other samples  $\,$ are characterized by local inclusions of CaO. Other observed effects such as anhydrite and fluorite formation and dissolution processes are common for all samples, which mean that these processes take place in the range of 307–481 °C. These changes are particularly observable at 10–45 μm scale, as confirmed by μCT on Ø8 mm core plugs.



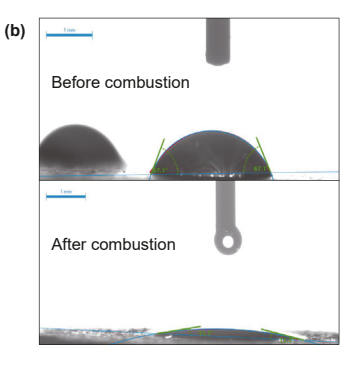


Fig. 14. (a) Mean contact angle values of different samples and (b) analysis of water droplet morphology for sample #15 before and after combustion experiment.

Initial carbonate rock	Carbonate rock after combustion	Effect
Calcite CaCO <sub>3</sub>	CaCO <sub>3</sub> , CaO and CO <sub>2</sub>	Decomposition of calcite   Increase in porosity and specific surface
Dolomite CaMg(CO <sub>3</sub> ) <sub>2</sub>	CaMg(CO <sub>3</sub> ) <sub>2</sub> , CaO, MgO and CO <sub>2</sub>	Decomposition of dolomite
_	- Anhydrite CaSO₄ - Fluorite CaF₂	Formation of new minerals:  - Anhydrite due to presence of S-containing compounds and CaO as part of calcite decomposition - Fluorite due to decomposition of the fluorine-containing cement  Decrease in local porosity Increase in specific surface
_	Fractures due to thermal expansion	Increase in <b>porosity</b>
_	Dissolution of calcite and dolomite	Increase in <b>porosity</b>

Fig. 15. Summary on observed mineral alterations and their effect on petrophysical properties.

#### 5.2. Change in porosity and pore size distribution

Transformation of the mineral matrix during high-temperature treatment is a multifaceted process that involves both a reduction in porosity and the creation of new pore space. This occurs through the number of processes such as dissolution and destruction of minerals, formation of new fractures and micropores that affect the overall pore connectivity and total porosity (Fig. 15). These alterations are proven by results of the drop shape analysis and low-temperature nitrogen adsorption. Increase in the total porosity is observed by all employed techniques (NMR/LS and  $\mu$ CT at 5  $\mu$ m/voxel) and can be explained by the mineral dissolution and destruction of grain contacts after the thermal stress relief (Table 7).

Accurate characterization of the rock porosity pre- and post combustion requires a combined application of several methods since each of them has a certain range of registered pore sizes (Fig. 16) due to the technical limitations.

The most reliable results for porosity and pore size evaluation in current study are provided by joint NMR/LS workflow since the computed tomography does not register the pores less than 5 µm size. However, computed tomography can reveal the appearance of large fractures, evaluate the homogeneity of the rock and provide a preliminary estimation of changes in open and closed porosity. Porosity by LS/NMR demonstrates the steady increase since both techniques are based on registration of the open connected pore space occupied by the injected fluid. NMR values prevail over the LS

**Table 7** Change in porosity and specific surface for selected core samples.

Sample ID	Parameter		Before combustion	After combustion	The change, %
#12	Porosity	LS, %	15.60	17.86	14
	•	NMR, %	18.44	22.88	24
		X-ray μCT, %	13.20	16.40	29
	Specific surface, n	n²/g	0.35	0.70	100
#15	Porosity	LS, %	20.24	21.25	5
	-	NMR, %	23.08	26.21	13
		X-ray μCT, %	15.40	12.00	-22
	Specific surface, n	n <sup>2</sup> /g	0.30	0.80	166
#20-1	Porosity	LS, %	14.97	15.82	5
		NMR, %	17.20	19.92	15
		X-ray μCT, %	17.60	17.00	-3
	Specific surface, n	n <sup>2</sup> /g	0.30	0.95	216

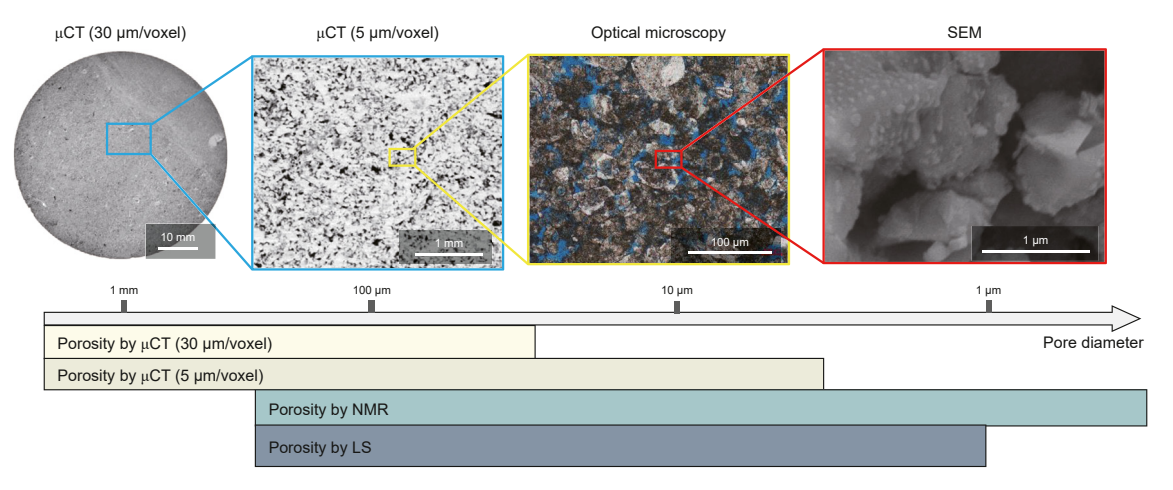


Fig. 16. Schematic application scale of techniques used for porosity and pore size determination for target samples.

results because the NMR also acquires the signal from closed pores and pores occupied by residual hydrocarbons and hydroxyl groups. It is notable that tomography shows smaller total porosity for some of the post combustion samples (#15 and #20-1). It can be explained by compaction and destruction of the pore space in the range of larger (macro pores) that contribute most to the result of the tomography measurement. This hypothesis is confirmed by the shift of the  $T_{2lm}$  by NMR and entire pore size distribution (Fig. 11) to the region of smaller pore sizes. Therefore, although the total porosity is higher in post combustion samples, the structure of the new porous space is modified and pore size histograms are significantly altered. The results of the BET analysis reflect the transformation of both the porous space and matrix, demonstrating an average 1.6 times increase in specific surface area for selected samples (Table 7).

#### 5.3. Wettability alteration and future implications for CO<sub>2</sub> storage

After combustion, wettability of target samples shifts from water-wet to strongly water-wet. This significant shift in the wettability of the samples can be attributed to the desorption of carboxylic acids and heavy oil fractions from the carbonate surface (Al-Hadhrami and Blunt, 2001). Crude oils, particularly heavy oils, often contain considerable amounts of high molecular weight compounds such as asphaltenes and resins and a high concentration of carboxylic acids. These components adhere to pore surfaces after oil migration, modifying the carbonate surface wetness to less hydrophilic. However, heavy oil fractions and specific carboxylic acids (e.g., palmitic, stearic, naphthenic) decompose at temperatures of 250–500 °C and 160–400 °C, respectively. Since the in-situ combustion experiments operated at 307-481 °C temperatures, most of these components underwent thermal decomposition, leading to a pronounced water-wet character of the carbonate surface. In addition, the increased surface roughness due to the formation of calcite crystals appears not to have influenced an increase in the droplet contact angles, suggesting that the water droplets are in the Wenzel state.

This transition alters the system's relative permeability, affecting the drainage and imbibition processes. In situations, where upgraded oil remains behind the combustion front, improved spontaneous imbibition may further reduce residual oil saturation. Additionally, post-combustion hydrophilic reservoir

with increased porosity could be considered for repurposing for  $CO_2$  storage. Oil-wet and mixed-wet conditions offer lower  $CO_2$  storage capacity than water-wet systems (Iglauer et al., 2015). Conversely, in hydrophilic macropores with  $CO_2$  as the non-wetting phase, water migration to narrow throat areas can trap gas in larger pores (capillary trapping), an effect less pronounced in mixed to oilwet systems, resulting in lower  $CO_2$  storage capacity (Alhosani et al., 2020). However, further experimental validation, focusing on extended  $CO_2$  flooding tests under reservoir conditions, is essential to quantify and compare  $CO_2$  storage capabilities pre- and post-combustion.

#### 6. Conclusions

In summary, we can highlight the most important outcomes as below:

- Petrographic analysis of the thin sections does not demonstrate any critical changes in the rock microtexture at the scale of optical microscopy. In turn, XRD shows a systematic decrease in dolomite and formation of a new mineral—anhydrite. Formation of anhydrite is associated with the calcite decomposition, observed by means of SEM as result of high-temperature in-situ combustion.
- 2) The SEM images illustrate alterations of mineral matrix: dissolution and destruction of calcite minerals, formation of new crystals of CaO, CaF<sub>2</sub> (fluorite) and CaSO<sub>4</sub> (anhydrite), microfractures and new pores at the scale of 5–10  $\mu$ m. Newly formed crystals are less than 1  $\mu$ m in size and can contribute to the change in reservoir properties. Samples, exposed to higher temperatures in the combustion experiment, demonstrate more pronounced alteration of calcite crystals with the formation of CaO.
- 3) Total porosity by NMR and gravimetric measurements (LS) increased in average for 15–20 rel.%. Based on X-ray μCT tomography images, the closed porosity decreased and open porosity showed greater values, which is directly related to the formation of new pores in the process of *in-situ* combustion. However, it is recommended to employ NMR/LS technique for evaluating the porosity and pore size due to the limited resolution of the μCT.

- 4) NMR results reveal the major changes in void space structure in the range from 1 to 30 μm in pore size distribution. In addition, all registered changes lead to 1.6 times increase in specific surface area, which is confirmed by results of the BET analysis. Wettability assessment demonstrates a shift to the strong water-wet behavior for post combustion samples, which can be explained by the thermal decomposition of heavy hydrocarbons.
- 5) In summary, the analysis of experimental results confirmed alterations in reservoir properties, including porosity, pore size distribution, specific surface, wettability, and the transformation of the rock mineral matrix. These modifications may substantially enhance the understanding of thermal combustion effects in carbonate reservoirs and help in calibration of field-scale numerical models for *in-situ* combustion. In addition, understanding these effects is the prerequisite for utilizing thermally treated reservoirs post-depletion, including CO<sub>2</sub> storage. However, further experimental studies must be designed to evaluate carbonate wettability under reservoir conditions, examine the chemical interactions between CO<sub>2</sub> and rock, and conduct long-term CO<sub>2</sub> flooding tests to quantify the reservoir's CO<sub>2</sub> storage and sealing capacity.

#### **Funding**

This research was supported by the Ministry of Science and Higher Education of the Russian Federation under agreement No. 075-10-2022-011 within the framework of the development program for a world-class Research Center.

#### **CRediT authorship contribution statement**

Aliya Mukhametdinova: Writing — original draft, Investigation, Data curation, Conceptualization. Tagir Karamov: Investigation, Writing — original draft. Strahinja Markovic: Data curation, Investigation, Writing — original draft. Andrey Morkovkin: Investigation, Methodology. Aleksander Burukhin: Formal analysis, Investigation. Evgeny Popov: Conceptualization, Data curation, Methodology. Zi-Qi Sun: Writing — original draft, Data curation, Methodology. Ren-Bao Zhao: Writing — original draft, Methodology, Conceptualization. Alexey Cheremisin: Writing — original draft, Supervision, Data curation, Conceptualization.

#### **Declaration of competing interest**

Aliya Mukhametdinova reports financial support was provided by Ministry of Science and Higher Education of the Russian Federation.

#### Acknowledgments

The authors are grateful to their colleagues from Skolkovo Institute of Science and Technology — Inna Chapanova for help with experimental studies and Dr. Natalia Sokolova for conducting low-temperature nitrogen adsorption tests. Finally, authors thank anonymous peer reviewers for their time and effort to make this paper better.

#### Appendix A. : Figures

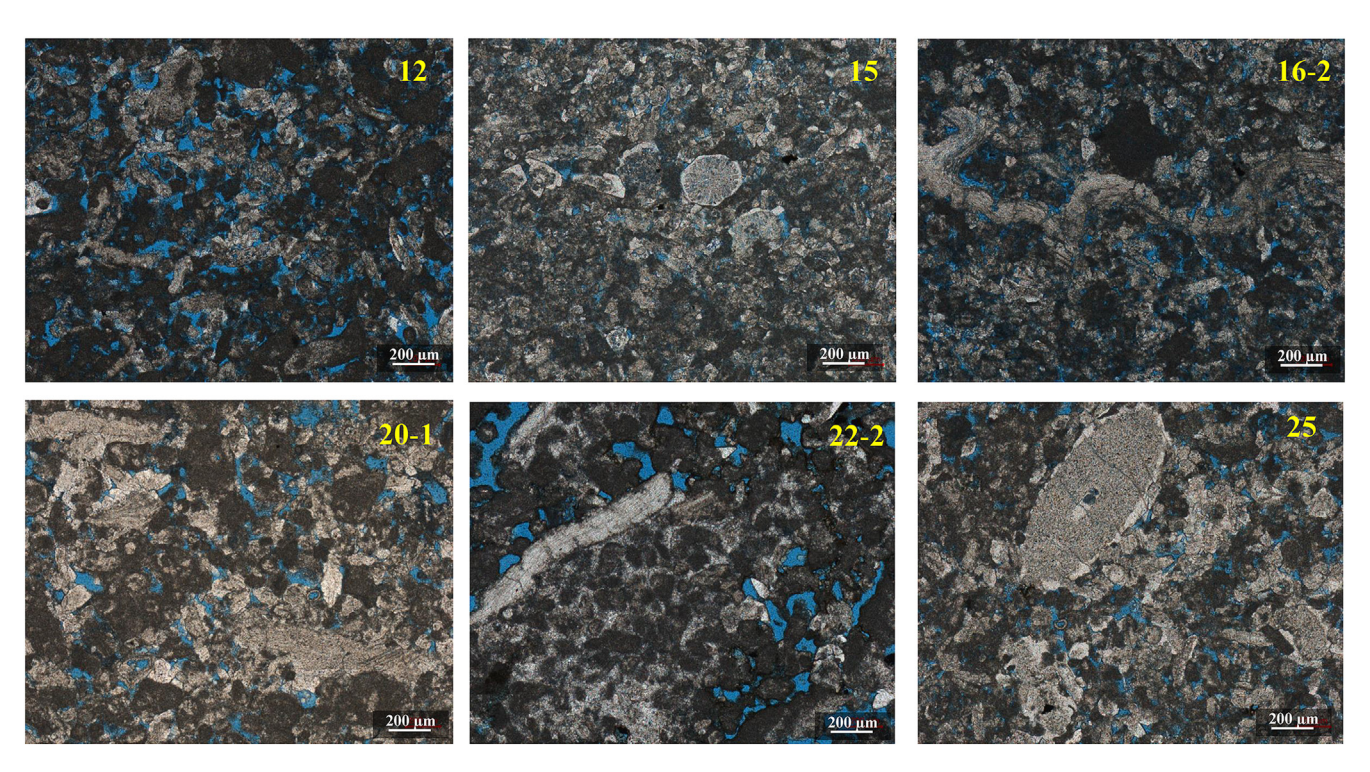


Fig. 17. Microphotographs of investigated grainstone after the experiment. The rock samples are identical to initial samples by means of optical microscopy.

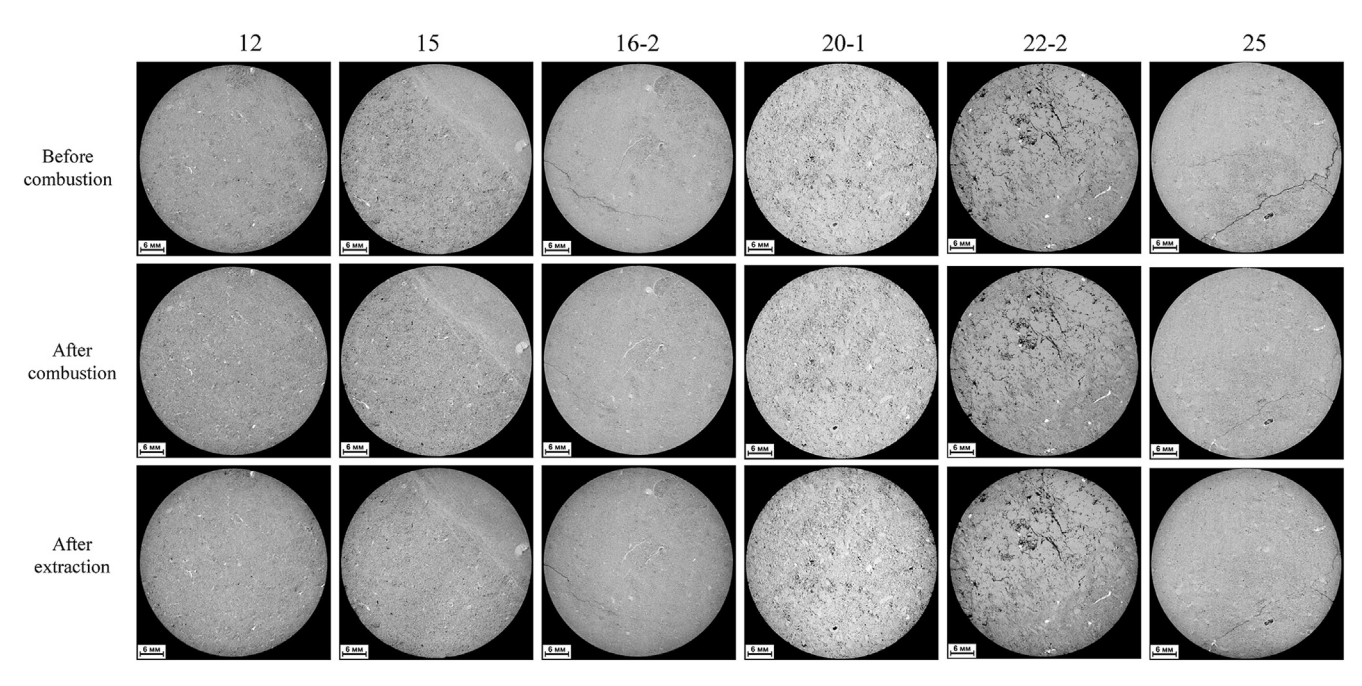


Fig. 18. Slices of 3D X-ray μCT images for Ø50 mm samples.

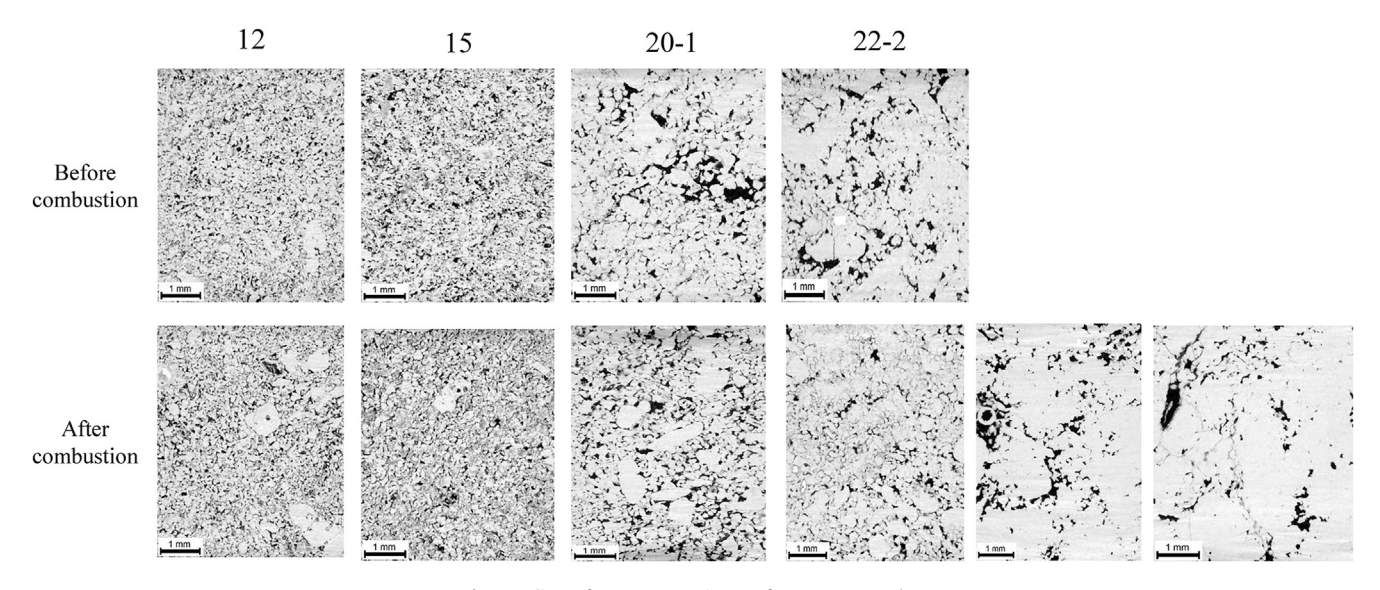


Fig. 19. Slices of 3D X-ray  $\mu CT$  images for Ø8 mm samples.

#### References

- Al-Hadhrami, H.S., Blunt, M.J., 2001. Thermally induced wettability alteration to improve oil recovery in fractured reservoirs. SPE Reservoir Eval. Eng. 4 (3), 179–186. https://doi.org/10.2118/71866-PA.
- Alanazi, A., Baban, A., Ali, M., Keshavarz, A., Iglauer, S., Hoteit, H., 2023. Residual trapping of CO<sub>2</sub>, N<sub>2</sub>, and a CO<sub>2</sub>-N<sub>2</sub> mixture in Indiana limestone using robust NMR coreflooding: implications for CO<sub>2</sub> geological storage. Fuel 353, 129221. https://doi.org/10.1016/j.fuel.2023.129221.
- Aleksandrov, D., Hascakir, B., 2015. Laboratory screening tests on the effect of initial oil saturation for the dynamic control of *in-situ* combustion. Fuel Process. Technol. 130, 224–234. https://doi.org/10.1016/j.fuproc.2014.10.027.
- Alexander, J.D., Martin, W.L., Dew, J.N., 1962. Factors affecting fuel availability and composition during *in situ* combustion. J. Petrol. Technol. 14 (10), 1154–1164. https://doi.org/10.2118/296-PA.
- Alhosani, A., Scanziani, A., Lin, Q., Raeini, A.Q., Bijeljic, B., Blunt, M.J., 2020. Porescale mechanisms of CO<sub>2</sub> storage in oilfields. Sci. Rep. 10 (1), 8534. https://

#### doi.org/10.1038/s41598-020-65416-z.

- Ariskina, K.A., Ding, Z., Abaas, M., Yuan, C., Emelianov, D.A., Chen, Q., Varfolomeev, M.A., 2021. Influence of carbonate minerals on heavy oil oxidation behavior and kinetics by TG-FTIR. Energies 14. https://doi.org/10.3390/ en14238136.
- Askarova, A., Turakhanov, A., Markovic, S., Popov, E., Maksakov, K., Usachev, G., Karpov, V., Cheremisin, A., 2020. Thermal enhanced oil recovery in deep heavy oil carbonates: experimental and numerical study on a hot water injection performance. J. Petrol. Sci. Eng. 194, 107456. https://doi.org/10.1016/j.petrol.2020.107456.
- Askarova, A.G., Popov, E.Y., Maerle, K.V., Cheremisin, A.N., 2022. Comparative study of in-situ combustion tests on consolidated and crushed core. SPE Reserv. Eval. Eng. 1–13. https://doi.org/10.2118/212270-PA.
- Barzin, Y., Moore, R.G., Mehta, S.A., Ursenbach, M.G., Tabasinejad, F., 2010. Impact of distillation on the combustion kinetics of high pressure air injection (HPAI). In: SPE Improved Oil Recovery Symposium. https://doi.org/10.2118/129691-MS.
- Bazargan, M., Chen, B., Cinar, M., Glatz, G., Lapene, A., Zhu, Z., Castanier, L., Gerritsen, M., Kovscek, A.R., 2011. A combined experimental and simulation

- workflow to improve predictability of in situ combustion. In: SPE Western North American Region Meeting, https://doi.org/10.2118/144599-MS
- Becattini, V., Motmans, T., Zappone, A., Madonna, C., Haselbacher, A., Steinfeld, A., 2017. Experimental investigation of the thermal and mechanical stability of rocks for high-temperature thermal-energy storage. Appl. Energy 203, 373–389. https://doi.org/10.1016/j.apenergy.2017.06.025.
- Berna, H., Ross, C.M., Castanier, L.M., Kovscek, A.R., 2013. Fuel formation and conversion during in-situ combustion of crude oil. SPE J. 18 (6), 1217–1228. https:// doi org/10 2118/146867-PA
- Bogdanov, I.I., Entov, V.M., Stepanov, V.P., 1990. Thermal decomposition of carbonate rocks under *in situ* combustion. J. Eng. Phys. 58 (5), 644–650. https:// doi.org/10.1007/BF00873185.
- Burger, J.G., 1972. Chemical aspects of in-situ combustion heat of combustion and kinetics. Soc. Petrol. Eng. J. 12 (5), 410–422. https://doi.org/10.2118/3599-PA.
- Chen, H.K., Li, B.Q., Yang, J.I., Zhang, B.J., 1998. Transformation of sulfur during pyrolysis and hydropyrolysis of coal. Fuel 77 (6), 487-493. https://doi.org/10.1016/ \$0016-2361(97)00275
- Dabbous, M.K., Fulton, P.F., 1974. Low-temperature-oxidation reaction kinetics and effects on the in-situ combustion process. Soc. Petrol. Eng. J. 14 (3), 253-262. https://doi.org/10.2118/4143-PA.
- Dunham, R.J., Ham, W.E., 1962. Classification of carbonate rocks according to depositional texture. In: Classification of Carbonate Rocks—A Symposium, vol. 1. American Association of Petroleum Geologists, https://doi.org/10.1306/
- Erdman, N., Drenzek, N., 2013. Integrated preparation and imaging techniques for the microstructural and geochemical characterization of shale by scanning electron microscopy. In: AAPG Memoir, 102, pp. 7-14. https://doi.org/10.1306/ 13391700M1023581
- Fathy, A., Adila, A.S., Ahmed, S., Hassan, A.M., Al-Shalabi, E.W., Al Ameri, W., 2023. Effects of rock heterogeneity and wettability on CO2 mineralization during storage in UAE depleted carbonate gas formations. In: ADIPEC: D031S116R005. https://doi.org/10.2118/216674-MS.
- Geng, Y., Liang, W., Liu, J., Cao, M., Kang, Z., 2017. Evolution of pore and fracture structure of oil shale under high temperature and high pressure. Energy Fuels 31 (10), 10404-10413. https://doi.org/10.1021/acs.energyfuels.7b01071.
- GIT, 2014. GIT Systems and Lithometrix User Manual, R7.0.
- Gutierrez, D., Moore, R.G., Ursenbach, M.G., Mehta, S.A., 2012. The ABCs of in-situcombustion simulations: from laboratory experiments to field scale. J. Can. Petrol. Technol. 51 (4), 256-267. https://doi.org/10.2118/148754-PA.
- Hascakir, B., Kovscek, A.R., 2014. Analysis of in-situ combustion performance in heterogeneous media. In: SPE Heavy Oil Conference-Canada. https://doi.org/ 10.2118/170008-MS
- Iglauer, S., Al-Yaseri, A.Z., Rezaee, R., Lebedev, M., 2015. CO<sub>2</sub> wettability of caprocks: implications for structural storage capacity and containment security. Geophys. Res. Lett. 42 (21), 9279–9284. https://doi.org/10.1002/2015GL06578
- Ismail, N.B., Hascakir, B., 2017. Increased asphaltenes surface aids fuel formation with the presence of clays during in-situ combustion. In: SPE Annual Technical Conference and Exhibition. https://doi.org/10.1016/j.ces.2008.10.026.
- Kalia, N., Balakotaiah, V., 2009. Effect of medium heterogeneities on reactive dissolution of carbonates. Chem. Eng. Sci. 64 (2), 376-390. https://doi.org/ 10.1016/j.ces.2008.10.026.
- Karamov, T., White, V., Idrisova, E., Kozlova, E., Burukhin, A., Morkovkin, A., Spasennykh, M., 2022. Alterations of carbonate mineral matrix and kerogen micro-structure in Domanik organic-rich shale during anhydrous pyrolysis. Minerals 12 (7), 870. https://doi.org/10.3390/min12070870.
- Karunadasa, K.S.P., Manoratne, C.H., Pitawala, H.M.T.G.A., Rajapakse, R.M.G., 2019. Thermal decomposition of calcium carbonate (calcite polymorph) as examined by in-situ high-temperature X-ray powder diffraction. J. Phys. Chem. Solid. 134, 21-28. https://doi.org/10.1016/j.jpcs.2019.05.023.
- Khakimova, L., Askarova, A., Popov, E., Moore, R.G., Solovyev, A., Simakov, Y., Afanasiev, I., Belgrave, J., Cheremisin, A., 2020. High-pressure air injection laboratory-scale numerical models of oxidation experiments for Kirsanovskoye oil field. J. Petrol. Sci. Eng. 188, 106796. https://doi.org/10.1016/ j.petrol.2019.106796.
- Kozlowski, M.L., Punase, A., Nasr-El-Din, H.A., Hascakir, B., 2015. The catalytic effect of clay on in-situ combustion performance. In: SPE Latin American and Caribbean Petroleum Engineering Conference. https://doi.org/10.2118/177166-MS.
- Larson, E.B., Emmons, R.V., 2021. Dissolution of carbonate rocks in a laboratory setting: rates and textures. Minerals 11. https://doi.org/10.3390/min11060605.
- Li, Y.B., Lin, X., Luo, C., Hu, Z.M., Jia, H.F., Chen, J.T., Pu, W.F., 2021. A comprehensive investigation of the influence of clay minerals on oxidized and pyrolyzed cokes in in situ combustion for heavy oil reservoirs. Fuel 302, 121168. https://doi.org/ 10.1016/i.fuel.2021.121168.
- Mamora, D.D., Ramey, H.J.J., Brigham, W.E., Castanier, L.M., 1993. Kinetics of in Situ Combustion. Stanford University Press
- Manrique, E.J., Muci, V.E., Gurfinkel, M.E., 2007. EOR field experiences in carbonate

- reservoirs in the United States. SPE Reservoir Eval. Eng. 10 (6), 667–686. https:// doi.org/10.2118/100063-PA.
- Markovic, S., Bryan, J.L., Rezaee, R., Turakhanov, A., Cheremisin, A., Kantzas, A., Koroteev, D., 2022. Application of XGBoost model for in-situ water saturation determination in Canadian oil-sands by LF-NMR and density data. Sci. Rep. 12 (1), 13984. https://doi.org/10.1038/s41598-022-17886-6.
- McPhee, C., Reed, J., Zubizarreta, I., 2015. Core Analysis: a Best Practice Guide. Elsevier, Amsterdam, Netherlands.
- Meng, J., Chen, S., Wang, J., Chen, Z., Zhang, J., 2022. Development and application of carbonate dissolution test equipment under thermal, hydraulic, chemical coupling condition. Materials 15. https://doi.org/10.3390/ma15207383.
- Minakov, A.V., Meshkova, V.D., Guzey, D.V., Pryazhnikov, M.I., 2023. Recent advances in the study of in situ combustion for enhanced oil recovery. Energies 16. https://doi.org/10.3390/en16114266
- Mogensen, K., Masalmeh, S., 2020. A review of EOR techniques for carbonate reservoirs in challenging geological settings. J. Petrol. Sci. Eng. 195, 107889. https:// doi.org/10.1016/j.petrol.2020.107889.
- Moore, R.G., Mehta, S.A., Ursenbach, M.G., 2002. A guide to high pressure air injection (HPAI) based oil recovery. In: SPE/DOE Improved Oil Recovery Symposium. https://doi.org/10.2118/75207-MS.
- Mukhametdinova, A., Karamov, T., Popov, E., Burukhin, A., Kozlova, E., Usachev, G., Cheremisin, A., 2022, Reservoir properties alteration in carbonate rocks after insitu combustion. SPE Reservoir Eval. Eng. 1–18. https://doi.org/10.2118/212281-
- Mukhametdinova, A., Mikhailova, P., Kozlova, E., Karamov, T., Baluev, A., Cheremisin, A., 2020. Effect of thermal exposure on oil shale saturation and reservoir properties. Appl. Sci. 10 (24). https://doi.org/10.3390/app10249065.
- Nelson, T., McNeil, I., 1961, How to engineer an in-situ combustion project, Oil Gas I. 59 58-65
- Olszak-Humienik, M., Jablonski, M., 2015. Thermal behavior of natural dolomite. J. Therm. Anal. Calorim. 119 (3), 2239–2248. https://doi.org/10.1007/s10973-014-4301-6.
- PerGeos, 2018. PerGeos Software. Thermo Fisher Scientific website. Pope, C., Ismail, N.B., Hascakir, B., 2020. Impact of carbonates on reaction kinetics of a bitumen combustion. In: SPE Canada Heavy Oil Conference. https://doi.org/ 10.2118/199959-MS.
- Popov, E., Askarova, A., Mukhametdinova, A., Maksakov, K., Usachev, G., Darishchev, V., Mehta, S.A., Cheremisin, A., 2021. Evaluation of the applicability of in-situ combustion in a heavy oil carbonate field with high initial oil saturation. Petrol. Sci. Eng. 207, 109146. https://doi.org/10.1016/ j.petrol.2021.109146.
- Puntervold, T., Strand, S., Mamonov, A., Piñerez, I.D.T., 2023. Recovery Improvement, Chapter 3 - enhanced oil recovery by smart water injection in sandstone reservoirs. Gulf Professional Publishing, pp. 109-184. https://doi.org/10.1016/ B978-0-12-823363-4.00002-9
- Raza, A., Gholami, R., Rezaee, R., Han Bing, C., Nagarajan, R., Ali Hamid, M., 2017. Preliminary assessments of CO2 storage in carbonate formations: a case study from Malaysia. J. Geophys. Eng. 14 (3), 533. https://doi.org/10.1088/1742-2140/
- Rodriguez, F., Llamedo, M., Belhaj, H., Mendoza, A., Elraies, K.A., 2023. Workflow of the in situ combustion EOR method in Venezuela: challenges and opportunities. ACS Omega 8 (31), 28060-28079. https://doi.org/10.1021/acsomega.2c08059.
- Sarathi, P.S., 1999. In-situ Combustion Handbook Principles and Practices. National Petroleum Technology Office. U.S. Department of Energy, Tulsa, Oklahoma. https://doi.org/10.2172/3175.
- Straley, C., Rossini, D., Vinegar, H.J., Tutunjan, P., Morriss, C.E., 1997. Core analysis by low-field NMR. Log. Anal. 38, 84-94.
- Sygała, A., Bukowska, M., Janoszek, T., 2013. High temperature versus geomechanical parameters of selected rocks - the present state of research. J. Sustain. Min. 12 (4), 45-51. https://doi.org/10.7424/jsm130407.
- Valverde, J.M., Perejon, A., Medina, S., Perez-Maqueda, L.A., 2015. Thermal decomposition of dolomite under CO<sub>2</sub>: insights from TGA and in situ XRD analysis. Phys. Chem. 17 (44), 30162–30176. https://doi.org/10.1039/C5CP05596B.
- Yavuz, H., Demirdag, S., Caran, S., 2010. Thermal effect on the physical properties of carbonate rocks. Int. J. Rock Mech. Min. Sci. 47 (1), 94-103. https://doi.org/ 10.1016/j.ijrmms.2009.09.014.
- Yekeen, N., Padmanabhan, E., Sevoo, T.A.L., Kanesen, K.A.L., Okunade, O.A., 2020. Wettability of rock/CO2/brine systems: a critical review of influencing parameters and recent advances. J. Ind. Eng. Chem. 88, 1-28. https://doi.org/10.1016/ i.iiec.2020.03.021.
- Zheng, J., Huang, J., Tao, L., Li, Z., Wang, Q., 2020. A multifaceted kinetic model for the thermal decomposition of calcium carbonate. Crystals 10 (9), 849. https:// doi.org/10.3390/cryst10090849.
- Zhu, Z., Liu, C., Chen, Y., Gong, Y., Song, Y., Tang, J., 2021. In-situ combustion simulation from laboratory to field scale. Geofluids 2021, 8153583. https://doi.org/ 10.1155/2021/8153583.